This is a repository copy of *Simulation of Particle-Laden Pipe Flows with a Homogeneous Stationary Sediment Bed*.

White Rose Research Online URL for this paper:
http://eprints.whiterose.ac.uk/148878/

Version: Accepted Version

Proceedings Paper:

This is an author produced version of a paper presented at ICMF 2019.

Simulation of Particle-Laden Pipe Flows with a Homogeneous Stationary Sediment Bed

Derrick O. Njobuenwu, Michael Fairweather

School of Chemical and Process Engineering, University of Leeds

Leeds, LS2 9JT, United Kingdom

d.o.njobuenwu@leeds.ac.uk, m.fairweather@leeds.ac.uk

Abstract

The characteristics of particle-laden turbulent pipe flows with stationary variable homogeneous bed heights are studied using large eddy simulation coupled to discrete particle simulation, and compared to a reference full pipe flow. Homogeneous stationary sediment beds of various heights are investigated to mimic geometries with the presence of deposited particles that have formed a bed at the bottom of the pipe which are relevant to nuclear waste processing operations. The flat boundary formed by the bed is found to induce different degrees of secondary flows and modifications to the fluid turbulence statistics and particle dynamics. The results obtained are of direct relevance to the behaviour of the two-phase flows encountered during nuclear waste processing, and have implications for particle dispersion, agglomeration, deposition and bed formation, as well as particle re-suspension from beds, in pipe flows transporting such waste.

Introduction

During decommissioning of the UK's legacy nuclear waste, with similar wastes existing in a number of other countries, waste in temporary storage needs to be retrieved and transported to supplementary treatment facilities for pre-treatment prior to immobilisation and eventual permanent storage. Practitioners involved in this waste management process adopt several techniques to reduce waste volumes and improve the management of waste disposal. Minimising the waste volume results in high mass loading which is desirable to reduce processing costs, however, this causes the waste to become more concentrated in terms of the particle volume fraction, and undesirable particle agglomeration and particle settling processes become more of an issue. Also, during the transport and processing of particle-laden flows, or sludges, if the solid-liquid flow rate becomes too low to suspend all the solid particles in the flow then it is not uncommon for a stationary solid sediment bed to form at the bottom of the cross-section of the conveying channel or pipe. A solid bed in the base of a pipe is a troublesome phenomenon as it can lead to enhanced pipe erosion, plugging or complete pipe blockage. Particle deposition and bed formation can also lead to modifications in the designed fluid dynamics of the systems used in processing.

Several experimental and numerical studies (e.g. Eggels et al. 1994; Uijttewaal & Oliemans 1996; den Toonder & Nieuwstadt 1997; El Khoury et al. 2013) have been performed over the few past decades to gain a thorough understanding of the fundamentals of single-phase pipe flows and fully suspended (liquid-solid) flows in pipes. The works conducted on pipe flows where a stationary solid sediment bed exists are limited (e.g. Matoušek 2011), and most of the available works concern flows in straight semi-circular cross-sectioned ducts (e.g. Berbish et al. 2011; Larsson et al. 2011), with the main focus being in relation to bed transport in rivers and sewage systems. Others have been concerned with the determination of practical engineering correlations for the average Nusselt number and average Darcy friction factor in such flows. These papers did not, however, consider the effect of the presence of a sediment bed on the single-phase flow and turbulence fields, and the attendant effect of the modified single-phase flow characteristics on the dynamics of particle dispersion, agglomeration, deposition and bed formation. The study by Larsson et al. (2011), for example, was limited to flows in semi-circular ducts and focused on the turbulent driven secondary flows of Prandtl's second kind. The influence of different sediment bed heights on such flows has not been previously considered.

The modelling of turbulent fully suspended particle-laden flows in circular cross-section channels is complex, and the addition of stationary variable height homogeneous beds increase this complexity. Since this flow configuration, with the presence of solid beds, is encountered both in nature and in engineering practice, it is important to develop techniques that can predict the fully suspended flows above deposits, as well as the deposition process itself. Matoušek (2011) has shown that the majority of available slurry flow models do not account for the presence of a deposited bed below the flow.

The presence of a stationary smooth surface, used to idealise the upper surface of a bed, introduces a flat boundary that is seen by the flow, in contrast to the circular boundary in the case of full pipe flows. It is expected that this flat boundary will introduce turbulent driven secondary flows of Prandtl's second kind that are inherent in flows in square cross-sectioned ducts. In this work, therefore, is our intention to compare how the presence or absence of these secondary flows affects

the overall characteristics and behaviour of particle-laden turbulent flows.

Understanding the effect that a stationary bed has on a liquid flow and the suspended particles within it, and comparisons of the multiphase behaviour within a variety of pipe geometries, are the motivations for the work described in this paper. Therefore, we investigate these systems using a previously well-validated large eddy simulation (LES) coupled to a discrete particle simulation (Njobuenwu & Fairweather 2017).

Numerical Methods

A coupled Eulerian-Lagrangian approach is adopted. An Eulerian description of the continuous phase, in the context of large eddy simulation, is employed. In LES, the continuity and Navier-Stokes equations are spatially filtered so that the energy containing large-scale turbulent motions are directly solved for, whilst the scales smaller than the filter width, that is the sub-grid scales, are modelled. The filtered continuity and Navier-Stokes equations are given as (Bini & Jones 2008):

$$\frac{\partial \bar{u}_i}{\partial x_i} = 0 \tag{1}$$

$$\frac{\partial \bar{u}_i}{\partial t} + \bar{u}_j \frac{\partial \bar{u}_i}{\partial x_j} = -\frac{1}{\rho}\frac{\partial \bar{p}}{\partial x_i} + \frac{\partial \bar{\tau}_{ij}}{\partial x_j} - \frac{\partial \tau_{ij}^{sgs}}{\partial x_j} + \Pi \delta_{i3} \tag{2}$$

The tensors, $\bar{\tau}_{ij}$ and τ_{ij}^{sgs}, are the viscous and the unknown sub-grid scale tensors, with the latter, which represents the effect of the sub-grid scale motions on the resolved motions, closed using the dynamically calibrated version of the Smagorinsky model (Germano et al. 1991; Piomelli & Liu 1995). In these equations, the source term Π is the mean pressure gradient imposed that drives the flow and δ_{i3} is the Kronecker function ($\delta_{ij} = 1$ for i = j, $\delta_{ij} = 0$ for $i \neq j$).

The LES was coupled with a Lagrangian particle tracking approach for the dispersed phase, where the motion of a particle in a turbulent flow is obtained from $\mathrm{d}\mathbf{x}_p = \mathbf{v}\mathrm{d}t$, with $\mathbf{v}$ given by:

$$\mathrm{d}\mathbf{v} = \left\{ \frac{(\bar{\mathbf{u}} - \mathbf{v})}{\tau_p} f_D + C_{SL} \frac{3\rho}{4\rho_p}[(\bar{\mathbf{u}} - \mathbf{v}) \times \bar{\boldsymbol{\omega}}] + \frac{\rho}{\rho_p}\frac{\mathrm{D}\bar{\mathbf{u}}}{\mathrm{D}t} \right.$$
$$\left. + \frac{\rho}{2\rho_p}\left(\frac{\mathrm{d}\bar{\mathbf{u}}}{\mathrm{d}t} - \frac{\mathrm{d}\mathbf{v}}{\mathrm{d}t}\right)\right\}\mathrm{d}t \tag{3}$$
$$+ \left(C_0 \frac{k_{sgs}}{\tau_t}\right)^{0.5}\mathrm{d}\mathbf{W}_t$$

Here, the derivatives $\mathrm{d}/\mathrm{d}t = \partial/\partial t + \mathbf{v} \cdot \nabla\bar{\mathbf{u}}$ and $\mathrm{D}/\mathrm{D}t = \partial\bar{\mathbf{u}}/\partial t + \bar{\mathbf{u}} \cdot \nabla\bar{\mathbf{u}}$ represent Lagrangian derivatives, following the particle and the containing fluid element, respectively, and boldface symbols denote vector quantities. The terms on the right-hand side of the equation are, respectively, contributions from the drag, shear lift, pressure-gradient and added mass forces, and a stochastic force term accounting for the influence of the sub-grid scale fluid velocity fluctuations on particle acceleration (Bini & Jones 2008; Njobuenwu & Fairweather 2017). The terms $\mathbf{v}$ and $\mathbf{x}_p$ are the particle instantaneous velocity and position, and $\bar{\mathbf{u}}$ and $\bar{\boldsymbol{\omega}} = 0.5(\nabla \times \bar{\mathbf{u}})$ are the known resolved fluid velocities and rotation interpolated at the particle position. The terms f_D and C_{SL} are, respectively, the drag and shear lift forces terms taken from the Schiller and Naumann drag correlation (Clift et al. 1978) and the Mei (1992) shear lift force correlation, both due to the particles' finite Reynolds number.

For the stochastic term, $C_0 = 1$ is a dispersion coefficient (Bini & Jones 2007) and the unresolved kinetic energy, $k_{sgs} = 2\Delta^2 C_S^{2/3}\bar{S}_{ij}\bar{S}_{ij}$, of the continuous phase is computed assuming equilibrium of the small scales. The term $d\mathbf{W}_t = \boldsymbol{\xi} \times \sqrt{dt}$ is the incremental Wiener term, where $\boldsymbol{\xi}$ is a random vector sampled with zero mean and a variance of unity, independently for each time step. The parameters Δ, C_S and $\bar{S}_{ij}$ are the filter width, Smagorinsky constant and filtered strain tensor, respectively. The interaction between particles and fluid phase turbulence is considered by the time scale, $\tau_t = \tau_p$. Other alternative time scales are reported in Bini & Jones (2007).

The BOFFIN-LES code (Bini & Jones 2008) was used to solve the descriptive fluid dynamic equations. The BOFFIN code implements Cartesian velocity components and a boundary conforming general curvilinear coordinate system with a co-located variable storage arrangement. It is based on a fully implicit low Mach number formulation and is second-order accurate in space and time. For the momentum equation convection terms, an energy-conserving discretisation scheme is used. All other spatial derivatives are approximated by standard second-order central differences. Time derivatives are approximated by a three-point backward difference scheme with a variable time step to ensure that the maximum Courant number, based on the filtered velocity, always lies between 0.1 and 0.2. A two-step, second-order, time-accurate approximate factorisation method (Rhie & Chow 1983) is applied to determine the pressure and ensure mass conservation in conjunction with a pressure smoothing technique to prevent even-odd node uncoupling of the pressure and velocity fields. The system of algebraic equations resulting from the discretisation is solved using a matrix preconditioned conjugate gradient method for the matrix of velocity vectors (van der Vorst 1992), and the incomplete Cholesky-conjugate gradient method for the pressure (Kershaw 1978).

The particle equations of motion were integrated using a fourth-order Runge-Kutta scheme, with a trilinear interpolation scheme used to obtain the instantaneous fluid velocity, velocity gradient, sub-grid scale kinetic energy and turbulence energy dissipation rate at a particle's position. The particles' initial position at the start of a simulation was random, and the initial velocity was set equal to that of the fluid at the particle's position.

Periodic boundary conditions were imposed in the streamwise direction for both the fluid flow and the particles, making it possible to prolong the duration of

the flow by continuous recirculation of the fluid and particles back into the domain, with a no-slip condition used at the walls and the simulated bed surface. For particle-wall and surface interactions, the perfect elastic collision condition was adopted such that all collisions resulted in a rebound back into the computational domain with no loss of kinetic energy. Further details of the numerical, initial and boundary conditions can be found in Bini & Jones (2008) and Njobuenwu & Fairweather (2017).

The flow was characterised by its shear Reynolds number, $Re_\tau = u_\tau R/\nu$, based on the shear velocity, u_τ, the radius of the full pipe, R, and the kinematic viscosity, ν. LES was carried out for the flow of an incompressible viscous fluid in a smooth circular pipe with varying bed heights, $B_h = 0, 1/4$ and $1/2$, representing full pipe, three-quarter pipe and half-pipe flows in the turbulent regime at four different shear Reynolds numbers $Re_\tau = 180, 360, 550$ and $1,000$. The pipe flow with bed height $B_h = 1/2$ is equivalent to the horizontal smooth semi-circular cross-sectioned duct flow found in the literature, and noted earlier. The pipe was populated with spherical particles with a fixed particle Stokes number based on the viscous scale of $St = 5$.

Results and Discussion

To demonstrate that the flow structures are preserved, the instantaneous velocity and vorticity profiles in a cross-sectional plane of the pipe are visualised and presented. Figure 1 shows cross-sections of the instantaneous streamwise velocity for the four shear Reynolds number pipe flows at $Re_\tau = 180, 360, 550$ and 1000 for the full pipe case. It is evident from the two-dimensional visualisation that flow structures become smaller as the fluid Reynolds number increases from $Re_\tau = 180$ in Figure 1(a) to $Re_\tau = 1000$ in Figure 1(d). In addition, the size of the characteristic mushroom shaped structures, or mushroom-eddies, in the pipe near-wall region reduces significantly with increases in Reynolds number. This observation is consistent with that obtained with direct numerical simulation (El Khoury et al. 2013).

Figure 2 shows the instantaneous streamwise vorticity of the four shear Reynolds number flows. Similar to the observations made in relation to Figure 1, the counter-rotating vortical structures near the pipe wall are clearly seen and their size becomes smaller with increases in the shear Reynolds number from $Re_\tau = 180$ to 1000. Also, from Figure 1, we can observe the small-scale near-wall structures that correspond to the streamwise low- and high-speed streaks, as well as the large-scale turbulent structures in the outer regions of the flow. Figure 3 also shows the low-speed-streaks at $x^+{\sim}10$ from the pipe boundary for shear Reynolds number $Re_\tau = 180$, and for the full pipe, $B_h = 0$, three quarter-pipe, $B_h = 1/4$, and half-pipe, $B_h = 1/2$, flows. Thus, the streamwise velocity field in the laminar sub-layer and buffer regions of wall-bounded flows is organised into alternating and elongated, streamwise-orientated narrow streaks of high and low speed fluid. These streaks are caused by quasi-steady streamwise vortices, that is long, thin tubes of vorticity, that are orientated principally in the streamwise direction.
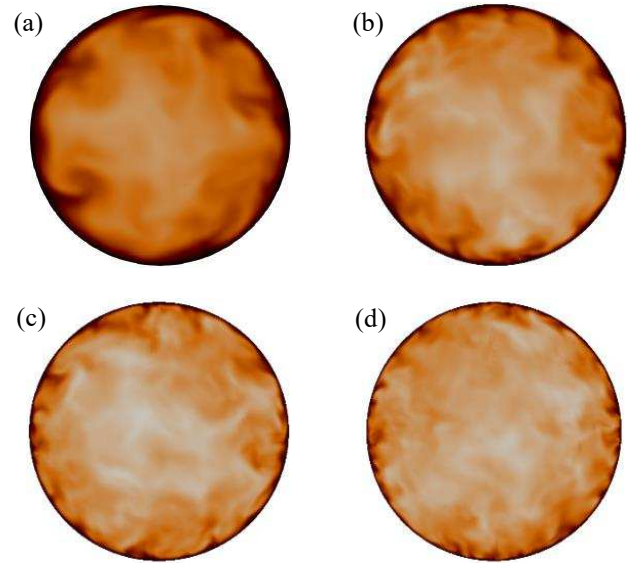

Figure 1: Pseudo-colour visualisation of the instantaneous streamwise velocity, $u_z^+ = u_z/u_\tau$, for (a) $Re_\tau = 180$, (b) $Re_\tau = 360$, (c) $Re_\tau = 550$ and (d) $Re_\tau = 1000$. Note, the colours vary from 0 (black) to 24 (white).

Figure 4 shows a validation of the LES predictions against available direct numerical simulation results (El Khoury et al. 2013) for the $Re_\tau = 180$ flow and the full pipe case. Good agreement is found in terms of the mean streamwise velocity, Figure 4(a), and the root mean square of the velocity fluctuations and the shear stress in Figure 4(b), confirming that the use of a highly resolved LES and dynamic modelling of the sub-grid scale term gives reliable results.
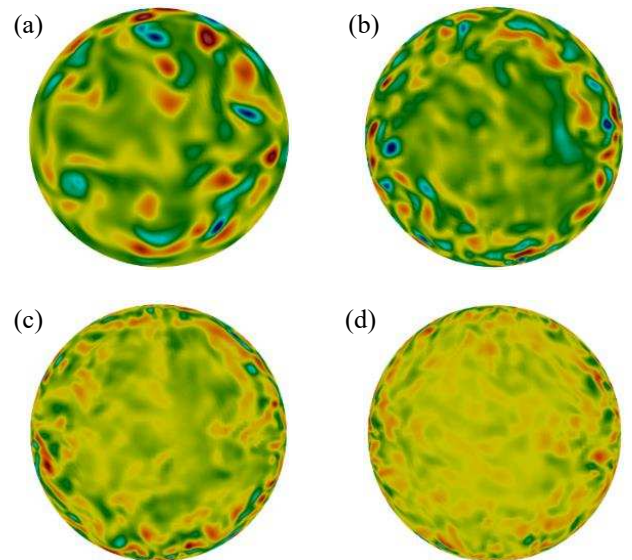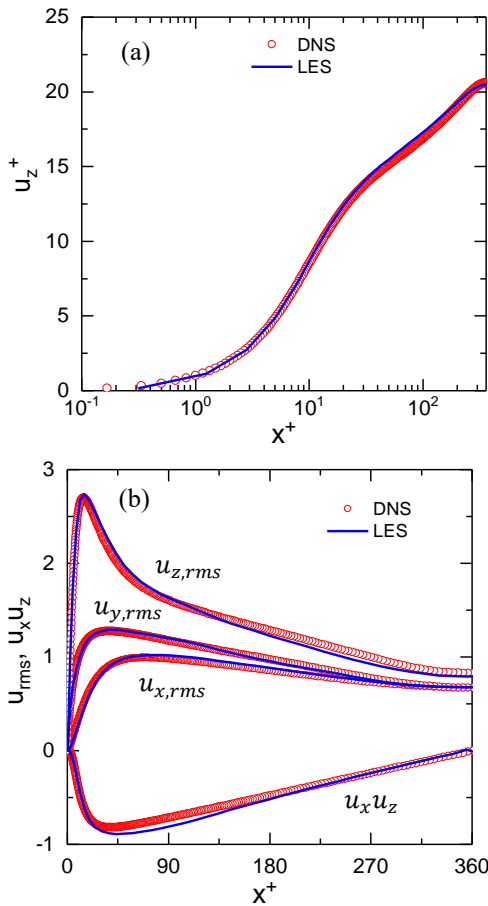

Figure 2: Pseudo-colour visualisation of the instantaneous streamwise vorticity, ω_z^+, for (a) $Re_\tau = 180$, (b) $Re_\tau = 360$, (c) $Re_\tau = 550$ and (d) $Re_\tau = 1000$. Note, red represents positive values and blue represents negative values.
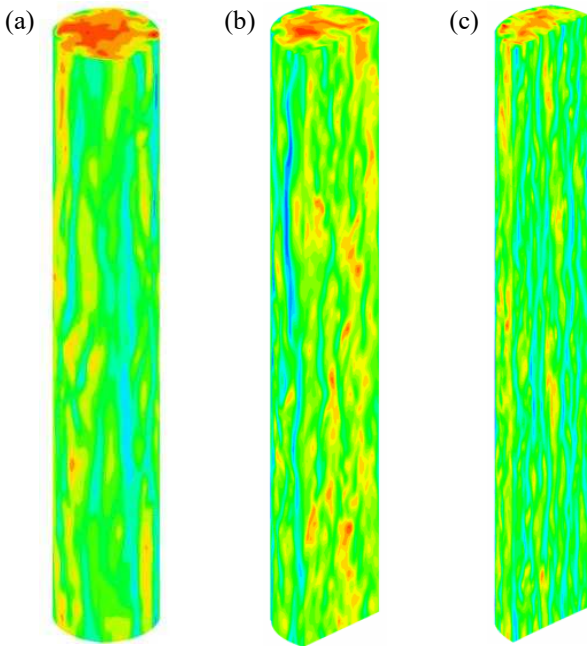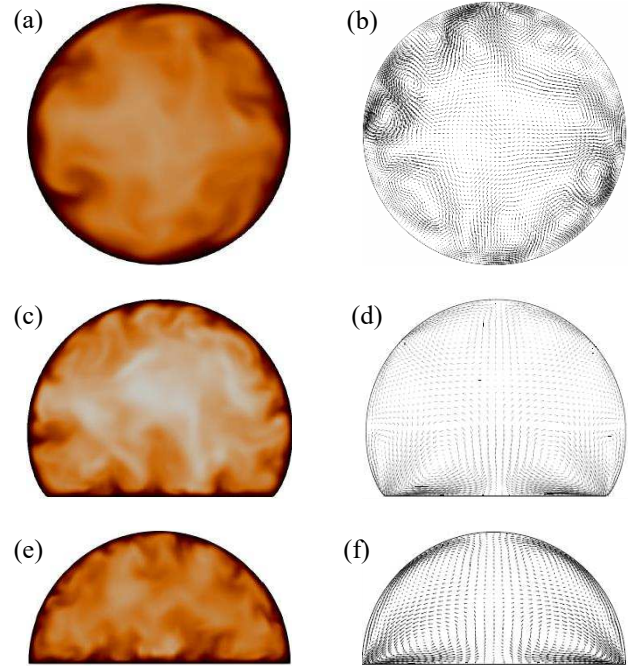
Figure 3: Low-speed-streaks at $x^+ \sim 10$ for shear Reynolds number $Re_\tau = 180$ for (a) full pipe flow, (b) three quarter-pipe flow, and (c) half-pipe flow.

Figure 4: Profiles of (a) mean streamwise velocity, u_z^+, and (b) turbulence intensities, u_{rms}, and Reynolds shear stress, $u_x u_z$, in inner scaling as a function of $x^+ = (1-r)^+$ at $Re_\tau = 180$ for bed height $B_h = 0$.
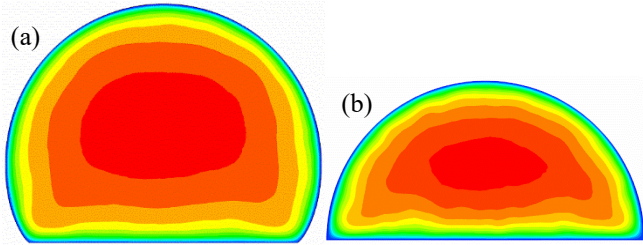

Figure 5: Visualisation of the turbulent pipe flow at shear Reynolds number, $Re_\tau = 180$, over a constant z-plane with (a, c, e) contours of instantaneous streamwise velocity normalised by the shear velocity, u_z^+, and (b, d, f) vectors of the mean velocity for (a, b) full pipe, $B_h = 0$, (c, d) three quarter-pipe, $B_h = 1/4$, and (e, f) half-pipe, $B_h = 1/2$.

The predicted instantaneous streamwise velocity for the various bed heights is shown in Figure 5(a, c, e). The size of the mushroom-eddies mentioned as occurring in the pipe near-wall region in Figure 1 are seen here to reduce significantly with an increase in the bed height from $B_h = 0$ in 5(a) to $B_h = 1/2$ in Figure 5(e). This is due to the presence of secondary flows, as shown in Figure 5(b, d, f), through velocity vector plots based on mean velocities at a cross-section along the streamwise direction, z-axis, for the full-pipe, the three quarter-pipe, and the half-pipe flow for shear Reynolds number $Re_\tau = 180$. There is an indication of the presence of secondary flows in Figure 5(d, f) due to the existence of the flat boundary arising from the simulated homogeneous stationary sediment bed, with no secondary flows seen in the full pipe flow in Figure 5(b), as would be anticipated. These secondary flows consist of two pairs of counter rotating corner vortices, with the flow convected into the corners of the pipe from the central region of the flow, and away from the corners along the pipe walls. The magnitude of the secondary flows is approximately 1-3% of the streamwise velocity. Even at such low values, the presence of the secondary flows still influences the characteristics of the mean flow and the turbulence structure, as seen in Figure 5(a, c, e), and is expected to have a significant influence on particle dynamics, including particle agglomeration and deposition.

Another indication of the existence of secondary flows in the pipes with stationary sediment beds is the distortion of the mean streamwise flow contours, shown in Figure 6 for $B_h = 1/4$ and $B_h = 1/2$, with these

cross sections obtained at the $N_z - 2$ node in the **z**-direction. This distortion due to the secondary flows causes the mean streamwise velocity contours to bulge out towards the corners of the pipe, with the degree of distortion increasing from the three quarter to the half pipe flow. Similar observations have been made by Larsson et al. (2011) in the case of semi-circular duct flows.

Figure 6: Pseudo-colour visualisation of the mean streamwise velocity of the turbulent pipe flow at shear Reynolds number, $Re_\tau = 180$, for (a) three quarter pipe, $B_h = 1/4$, and (b) half-pipe, $B_h = 1/2$. Note, red represents maximum values and blue represents minimum values (in this case zero).
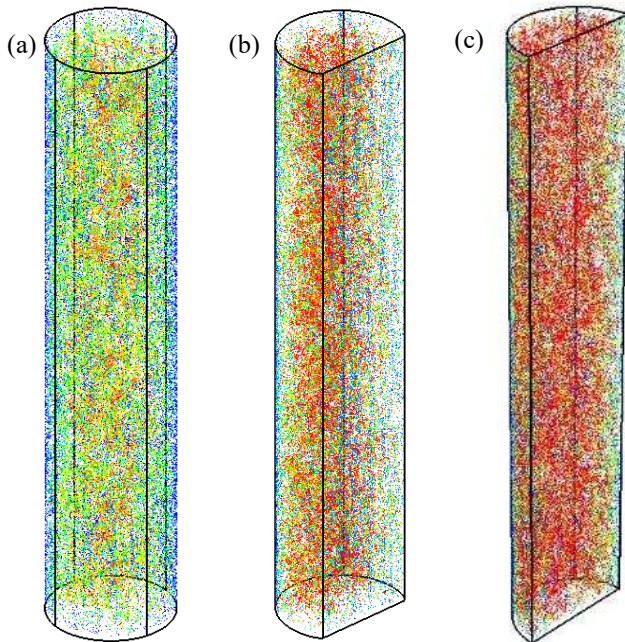

Figure 7: Snapshots of particle spatial distribution in the whole computational domain plotted in arbitrary aspect ratio. Particle dimeter is $d_p = 60\ \mu m$, Stokes number, $St = 5$: (a) full pipe, $B_h = 0$, (b) three-quarter, $B_h = 1/4$, and (c) half-pipe, $B_h = 1/2$.

A visual impression of particle locations within the whole computational domain is shown in Figure 7 for the pipe flow with various bed heights, this time at a shear Reynolds number, $Re_\tau = 360$, and for particle properties: diameter, $d_p = 60\ \mu m$, Stokes number, $St = 5$ and number of particles, $N_p = 100,000$. The figure shows typical three-dimensional particle spatial distributions, though not drawn to scale. The particle behaviour is influenced by the presence or absence of

the stationary flat bed, and the induced secondary flows, and turbophoretic effects, that is, the tendency for particles to migrate in the direction of decreasing turbulence levels which acts to segregate particles, inducing preferential accumulation of inertial particles at the pipe wall.

Further details are provided in Figure 8 where cross-flow slices for the three cases are plotted. The thickness of the slice is approximately $R/5$, and samples of the particles were taken at the exit of the pipe for all three cases. The figures show that more accumulation of the particles occurs on the curved pipe surface than on the flat bed surface. Hence, more particles are deposited in the case of the full pipe flow in Figure 8(a) than in Figure 8(b) for the three-quarter pipe flow or in Figure 8(c) for the semi-circular cross sectioned pipe. As the secondary flows were found to be stronger as the bed height increases, it is evident that these secondary flows have enhanced particle re-suspension from the solid flat surface back into the main body of the flow, resulting in fewer deposited particles.
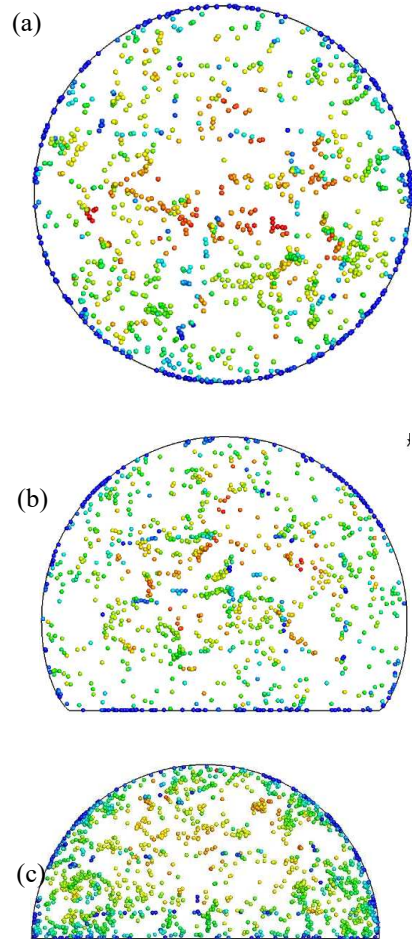
Figure 8: Instantaneous particle spatial distribution in a thin cross flow slice of thickness of $R/5$ for particle diameter $d_p = 60\ \mu m$ and Stokes number, $St = 5$ at shear Reynolds number, $Re_\tau = 360$: (a) full pipe flow, $B_h = 0$, (b) three-quarter pipe flow, $B_h = 1/4$, and (c) half pipe flow, $B_h = 1/2$ flow (Colour encoded for the particle instantaneous streamwise velocity, with blue as 0 and red as the maximum, the size of the shape is arbitrary).

Conclusions

Large eddy simulation of turbulent pipe flow with variable bed heights was performed to simulate various degrees of bed formation, representative of situations that may occur during the mobilisation and transport of nuclear waste. The results presented in this study reproduced the main features derived in studies on similar geometries (e.g. secondary flows in flows with sediment beds). Results from discrete particle simulation, coupled to the large eddy simulations, showed that particle deposition on the curved and flat surfaces occurs to different extents, largely due to the presence of secondary flows which enhance particle re-suspension from the solid flat surface. All these results are of relevance to the behaviour of the two-phase flows encountered during waste processing operations, and have wider implications for particle dispersion, agglomeration, deposition and bed formation, as well as particle re-suspension from beds, in pipe flows transporting waste.

Acknowledgements

References

Berbish, N. S., Moawed, M., Ammar, M. & Afifi, R. I. Heat transfer and friction factor of turbulent flow through a horizontal semi-circular duct. Heat Mass Transfer, Vol. 47, pp. 377-384 (2011)

Bini, M. & Jones, W. P. Particle acceleration in turbulent flows: A class of nonlinear stochastic models for intermittency. Phys. Fluids, Vol. 19, p. 035104 (2007)

Bini, M. & Jones, W. P. Large-eddy simulation of particle-laden turbulent flows. J. Fluid Mech., Vol. 614, pp. 207-252 (2008)

Clift, R., Grace, J. R. & Weber, M. E., Bubbles, drops and particles. Academic Press, New York (1978)

den Toonder, J. M. J. & Nieuwstadt, F. T. M. Reynolds number effects in a turbulent pipe flow for low to moderate Re. Phys. Fluids, Vol. 9, pp. 3398-3409 (1997)

Eggels, J. G. M., Unger, F., Weiss, M. H., Westerweel, J., Adrian, R. J., Friedrich, R. & Nieuwstadt, F. T. M. Fully developed turbulent pipe flow: A comparison between direct numerical simulation and experiment. J. Fluid Mech., Vol. 268, pp. 175-210 (1994)

El Khoury, G. K., Schlatter, P., Noorani, A., Fischer, P. F., Brethouwer, G. & Johansson, A. V. Direct numerical simulation of turbulent pipe flow at moderately high Reynolds numbers. Flow Turbul. Combust., Vol. 91, pp. 475-495 (2013)

Germano, M., Piomelli, U., Moin, P. & Cabot, W. H. A dynamic subgrid-scale eddy viscosity model. Phys. Fluids, Vol. 3, pp. 1760-1765 (1991)

Kershaw, D. S. The incomplete Cholesky-conjugate gradient method for the iterative solution of systems of linear equations. J. Comput. Phys., Vol. 26, 43-65 (1978)

Larsson, I. A. S., Lindmark, E. M., Lundström, T. S. & Nathan, G. J. Secondary flow in semi-circular ducts. J. Fluids Eng., Vol. 133, pp. 101206-101206-8 (2011)

Matoušek, V. Solids transport formula in predictive model for pipe flow of slurry above deposit. Particul. Sci. Technol., Vol. 29, pp. 89-106 (2011)

Mei, R. An approximate expression for the shear lift force on a spherical particle at finite Reynolds number. Int. J. Multiphas. Flow, Vol. 18, pp. 145-147 (1992)

Njobuenwu, D. O. & Fairweather, M. Simulation of deterministic energy-balance particle agglomeration in turbulent liquid-solid flows. Phys. Fluids, Vol. 29, p. 083301 (2017)

Piomelli, U. & Liu, J. Large-eddy simulation of rotating channel flows using a localized dynamic model. Phys. Fluids, Vol. 7, pp. 839-848 (1995)

Rhie, C. M. & Chow, W. L. Numerical study of the turbulent flow past an airfoil with trailing edge separation. AIAA J., Vol. 21, 1525-1532 (1983)

Uijttewaal, W. S. J. & Oliemans, R. V. A. Particle dispersion and deposition in direct numerical and large eddy simulations of vertical pipe flows. Phys. Fluids, Vol. 8, pp. 2590-2604 (1996)

van der Vorst, H. Bi-CGSTAB: A fast and smoothly converging variant of Bi-CG for the solution of nonsymmetric linear systems. SIAM J. Sci. Stat. Comput., Vol 13, pp. 631-644 (1992).